Dynamic properties of unstable motion of swirling premixed flames generated by a change in gravitational orientation

Hiroshi Gotoda[*]

Department of Mechanical Engineering, Ritsumeikan University, 1-1-1 Noji-higashi, Kusatsu, Shiga 525-8577, Japan

Takaya Miyano[†]

Department of Micro System Technology, Ritsumeikan University, 1-1-1 Noji-higashi, Kusatsu, Shiga 525-8577, Japan

Ian G. Shepherd

Combustion Group, Advanced Technologies Department, Environmental Energy Technologies Division,
Lawrence Berkeley National Laboratory, Berkeley, California 94720, USA

The dynamic behavior of swirling premixed flames generated by the effect of the gravitational orientation has been experimentally and numerically investigated. When the gravitational direction relative to the flame front is changed, i.e., in inverted gravity ($-1G$), an unstable flame is formed in a limited domain of equivalence ratio and swirl number. The time history of flame front fluctuation shows that high-energy chaotic motion is superimposed on a periodic oscillation generated by unstable vortex motion in the combustion products. This results in the dynamic motion of the unstable flame becoming deterministically chaotic. This is clearly demonstrated by sophisticated nonlinear time series analysis, which has not been widely applied to the investigation of combustion phenomena.

I. INTRODUCTION

Periodic and chaotic motion in flame dynamics that can be observed as a result of flame instabilities are of fundamental importance to present-day combustion physics and thermal fluid science research. The buoyant force driven by natural convection under terrestrial gravity is one of the most significant factors in the generation and growth of flame instabilities. There are two major flame instabilities generated by the upward buoyant force, i.e., normal gravity ($+1G$): (a) hydrodynamic shear layer instability associated with the Kelvin-Helmholtz instability and (b) the Rayleigh-Taylor instability. In open premixed flames, the entire flow field consists predominantly of cold dense reactants (heavy gas) in the upstream flow, hot combustion products (light gas) in the downstream flow, and cold surrounding air (heavy gas). When the hot combustion products accelerated by the upward buoyant force interact with the cold surrounding air, the interface between these fluids becomes unstable owing to the hydrodynamic shear layer instability, resulting in the formation of a large-scale toroidal vortex at the interface. This vortex produces periodic velocity fluctuations in the reactant flow through the pressure field and causes the flame front to oscillate at a distinct characteristic frequency (10–20 Hz) [1–4]. When one considers the $+1G$ gravitational direction relative to the flame front, the interface between the hot combustion products above the cold dense reactants is stable for flow perturbations, while in the inverted gravity ($-1G$) case, the interface is unstable owing to the Rayleigh-Taylor instability. By inverting the orientation of the burner system rela-

tive to the gravitational direction, light combustion products are formed below heavy reactants, and upward propagating flames become sensitive to the dynamic motion of the light combustion products. In fact, for lean premixed flames under low Reynolds number conditions (buoyancy-dominated region: Richardson number $R_i > 0.1$), the overall flame configuration in $-1G$ is significantly distorted [4,5]. The mean pressure gradient in hot combustion products suppresses the wrinkle formation of the flame front in normal gravity, while it amplifies wrinkling in inverted gravity [6]. The relevance of the Rayleigh-Taylor instability mechanism to the deformation of the flame front configuration and the effect of the gravitational direction is addressed, which have a significant impact on flame dynamics.

It is well known that swirling flow is one of the most important flow configurations in fundamental and practical combustion systems. In large practical swirl combustors, the effects of buoyancy on flame dynamics is smaller than those of the initial jet momentum and centrifugal force, because swirling flames are utilized under turbulent flow conditions. However, it is expected that the role of buoyancy will be significant under predominantly laminar flow conditions. Therefore, it is necessary to understand how the buoyancy/swirl interaction affects flame front dynamics when the gravitational direction relative to the flame front is changed.

With respect to experimental investigations of flame dynamics generated by swirling flow, a rotating burner that spins on its central axis is one of the most fundamental flame configurations [7–9]. This configuration makes it possible to independently and systematically control the centrifugal force and initial jet momentum. In our preliminary work using a rotating Bunsen burner [10], we observed that changes in the buoyancy/swirl interaction generated by the effect of the gravitational orientation may cause irregular fluctuations

*gotoda@se.ritsumei.ac.jp

†tmiyano@se.ritsumei.ac.jp

in flame front dynamics that are thought to be chaotic rather than turbulent. Revealing whether or not the dynamic behavior is deterministic chaos is significant for understanding the flame instability issue that arises in swirling combustion, which remains to be elucidated. A nonlinear time series approach inspired by chaos theory is becoming an increasingly reliable tool for clarifying the nonlinear properties of complex dynamics in a dissipative system. In the field of thermal and fluid science, nonlinear time series analysis has been widely applied in recent years to study the dynamic motion of forced transitional jets [11], the transition process of a separated shear layer [12], flow fluid motion in a heated air flow [13], the fluctuation features of two-phase flow [14], and relaminarization phenomena in a spherical Couette flow [15]. Regarding flame instability, we have recently demonstrated the suitability of nonlinear time series analysis for characterizing the dynamic behavior of nonperiodic oscillations in a diffusion flame [16]. In these works, a method to infer the fractal dimension in a constructed phase space, that is, the Grassberger-Procaccia method [17], is used to quantify the dynamic properties of time series data. This method is one of the most common prevalent and useful methods for characterizing dynamic properties, but it leads to misinterpretation and misdiagnosis in the quantification of dynamical properties when applied to time series data that is slightly affected by a stochastic process. To solve this problem, some sophisticated methods based on nonlinear forecasting and the parallelism of trajectories in phase space have been proposed as a powerful diagnostic method that can accurately extract the extent of determinism in complex dynamic behavior [18,19]. In fact, the importance of these methods has been addressed in previous works [20,21]. An investigation of the dynamic properties of flame instability observed in this study by sophisticated nonlinear chaos analysis is important for gaining a comprehensive understanding of complex nonlinear phenomena in flame dynamics. Nevertheless, this interesting issue has not yet been investigated extensively in the fields of combustion science and physics.

The main purpose of this study is to conduct a more comprehensive investigation of the dynamic behavior of the flame front generated by inversion of the gravitational direction under swirling flow conditions from the viewpoint of nonlinear dynamics. First, the changes in the overall flame shapes of swirling flames are experimentally investigated, and the formation region of an unstable flame is examined. The relevance of buoyancy to the dynamic motion of the unstable flame is discussed by visualizing hot combustion products behind the flame front. Next, the dynamic properties of the unstable flame are studied in greater detail by numerical analysis based on nonlinear time series analysis in combination with the surrogate method of time series data obtained from the fluctuating flame front. We utilize the mathematical methods devised by Sugihara and May [18] and by Wayland *et al.* [19] to reveal the extent of determinism in the flame dynamics. The statistical significance of the estimated statistics is evaluated by the surrogate method [22]. This paper is organized as follows. In Sec. II, the experimental system and the method used in this work are described. In Sec. III, we present the central ideas behind the mathematics of nonlinear time series analysis. Experimental
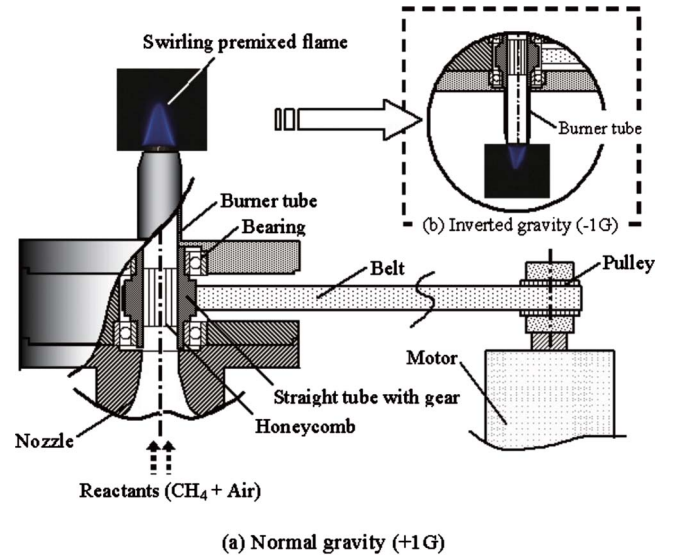
FIG. 1. (Color online) Schematic of burner system.

and numerical results are presented and discussed in Sec. IV. We present our conclusions in Sec. V.

II. EXPERIMENTAL APPARATUS AND PROCEDURE

The burner system we used in this study is shown schematically in Fig. 1. The premixed CH_4/air reactants flow through a diffuser, fine damping screens, a nozzle, a straight tube with a gear, and a burner tube. The straight tube has a diameter of 12 mm and is fitted on top of the nozzle, which is vertically supported by two bearings and rotated by a dc motor through a pulley and belt system. A 15-mm-thick honeycomb section with a grid diameter of 1.04 mm is fitted inside the straight tube to produce the solid-body rotation of the reactants at the burner tube exit [8]. The straight tube rotates in a counterclockwise direction viewed from the top. Unlike the burner system used in previous works [9,10], the surface of the burner tube in this work does not rotate (note that the solid-body rotation is given to the fuel flow without rotating the surface of the burner tube) in order to remove the effect of Taylor-like vortex motion around the burner tube exit generated by centrifugal instability [16]. The modification of the burner system alters the configuration and formation region of swirling flames reported in our previous works [9,10]; swirling flames formed above the modified burner exit are more suitable for applying nonlinear time series analysis to the dynamic behavior of the fluctuating flame front. The bulk flow velocity of the reactants U_0 (=volumetric flow-rate/cross-sectional area of the burner tube) was varied from 0.8 m/s (buoyancy-dominated region: $R_i > 0.1$) to 1.6 m/s (momentum-dominated region: $R_i < 0.1$). The Richardson number R_i, defined as $((T_{ad} - T_0)/T_{ad})(Gd_0/U_0^2)$, where T_{ad} is the adiabatic flame temperature, T_0 is the temperature of the surrounding air (300 K), G is gravitational acceleration, and d_0 is the diameter of the burner tube, can be used to distinguish flow conditions where buoyancy is significant, $R_i > 0.1$, from those where it is not significant, $R_i < 0.1$ [4,5]. The Reynolds number R_e
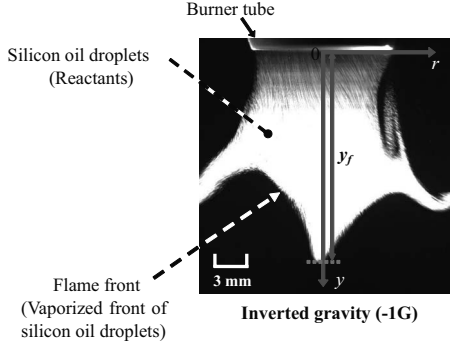
FIG. 2. Definition of flame front location.

based on the burner exit diameter is between 620 and 1250. The equivalence ratio of premixed reactants ϕ was varied from 0.60 to 0.90. The rotational speed of the straight tube N was varied from 0 to 5100 rpm (85 s^{-1}). To characterize the balance between axial momentum and swirl momentum, the Swirl number S is introduced using the following equation, and was varied from 0 to 1.0.

$$S = \frac{2\pi \int_0^{d_0/2} \rho u v_\theta r^2 dr}{2\pi \left(\frac{d_0}{2}\right) \int_0^{d_0/2} \rho u^2 r dr} = \frac{\omega d_0}{4U_0}, \tag{1}$$

Here, u is the axial velocity of the reactants, ρ is the density of the reactants, v_θ is the tangential velocity, and $\omega(=\pi N/30)$ is the angular velocity of the burner tube.

To investigate the dynamic properties of the flame front fluctuation of the unstable flame, a laser tomographic method is used. The continuous light source is a Nd:Yag (YV04) laser (Japan Laser DPGL 5W) with a maximum power of 5 W. An optical unit shapes the laser beam into a sheet with a thickness of approximately 0.5 mm, and the laser sheet then traverses the test section. Silicon oil droplets with diameters of $1-2$ μm are dispersed in the reactants as scatters. The Mie scattered light emitted from the droplets shows the region where the temperature is below $\sim$570 K; this region corresponds to the reactants. The upstream side of the preheat zone can then be visualized by observing the front of the silicon oil droplets [23]. The visualized images are recorded by a high-speed video camera (Photron 1024 PCI) at 1000 frames per second with a frame size of 1024×1024 pixels. The spatial resolution of the images is 27 pixels per millimeter, which is sufficient for analyzing the flame front motion. As shown in Fig. 2, the location of the vaporized front along the centerline of the burner tube is defined as the flame front location y_f(mm), and the deviation from the mean flame front location is $\Delta y_f = y_f - \bar{y}_f$. Here, $\bar{y}_f$ is the time-averaged flame front location as a function of time t and is measured to investigate the dynamic behavior of the unstable flame. To investigate how hot combustion products affect the dynamic behavior of the flame front, refractory TiO$_2$ particles are also dispersed in the reactants as scatters.

III. MATHEMATICAL TREATMENT USED FOR NONLINEAR TIME SERIES ANALYSIS

As mentioned in Sec. I, nonlinear time series analysis is important for gaining a comprehensive understanding of dynamic behavior in complex nonlinear phenomena. A standard and classical method for evaluating the complexity of dynamic behavior is the Grassberger-Procaccia (GP) algorithm, which enables the estimation of the correlation dimension of a geometrical object formed from trajectories in the phase space reconstructed from a time series [17]. This algorithm has been widely used in previous studies on combustion and fluid-dynamics instabilities [11–16,24]. Nonetheless, well-known flaws of the GP algorithm are that it is often distorted by colored noise [25] and that it yields false estimates when the amount of data available is small [26]. To circumvent this problem, we used the Sugihara-May (SM) algorithm [18] and that of Wayland *et al.* [19] instead of the GP algorithm. These algorithms may also be considered conventional, but they can provide reliable estimates from a short time series and are robust to the noise contamination of obtained data.

Recently, a method of nonlinear time series analysis involving a simple binary test has been developed by Gottwald and Melbourne [27] to distinguish chaotic processes from nonchaotic ones, referred to as the 0–1 test. Although this test is simple and nonparametric, we did not use it in this work. As shown in Sec. IV, the observed flame motion appears to be chaotic and superimposed on periodic motion. Hence, the question of whether the flame motion is chaotic or nonchaotic may be ill posed. In the following subsections, we briefly describe the central ideas behind the mathematics of each method of time series analysis employed in this work.

A. Mutual information

The mutual information defined below, introduced by Fraser and Swinney [28], is a function of the time distance between the data points of a time series and provides useful information for determining the optimal time lag for embedding [29] as well as for measuring the rate of spontaneous decay of information from the time series. Let U and V be sets of realizations of the random variables u and v, respectively. We approximate the probability density functions $p(u)$ and $p(v)$ and the joint probability density function $p(u,v)$ with one- and two-dimensional histograms generated from sets of sample data $\{u_i\}_{i=1}^n$ and $\{v_i\}_{i=1}^n$. Here, n is the number of samples. The information entropies $H(U)$ and $H(V)$ and the joint information entropy $H(U,V)$ are calculated using

$$H(U) = -\sum_{i=1}^n p(u_i) \log_2 p(u_i), \tag{2}$$

$$H(V) = -\sum_{i=1}^n p(v_i) \log_2 p(v_i), \tag{3}$$

$$H(U,V) = -\sum_{i,j=1}^{n} p(u_i, v_j) \log_2 p(u_i, v_j). \tag{4}$$

The average mutual information $I(V;U)$ is given by

$$I(V;U) = H(U) + H(V) - H(U,V). \tag{5}$$

Here, $I(V;U)$ represents the amount of information that one can know about V given U. In this work, the time series $\{\Delta y_f(t)\}_{t=1}^{n-\tau}$ is substituted into U and its time-delayed counterpart $\{\Delta y_f(t+\tau)\}_{t=1}^{n-\tau}$ is substituted into V. Then, the mutual information is a function of the time lag τ, denoted by I, and represents the spontaneous loss of information caused by the time evolution of the system in terms of τ. The exponential decay of I can indicate chaos.

B. Short-term predictability

The sensitivity of the time evolution of a system to small changes under initial conditions is a critical characteristic of chaos, which causes an exponential decay of predictability with time despite the determinism governing the dynamic behavior of the system. This effect is known as short-term predictability followed by long-term unpredictability, which is at the heart of the SM algorithm [18]. According to Takens' embedding theorem [29], we form D-dimensional vectors $\mathbf{x}(t)$ consisting of time-delayed sequences truncated from a time series as

$$\mathbf{x}(t) = \{\Delta y_f(t), \Delta y_f(t-\tau_0), \ldots, \Delta y_f[t-(D-1)\tau_0]\}, \tag{6}$$

where D is the embedding dimension and τ_0 is a suitable time lag. In this work, we determine τ_0 in accordance with the prescription of Fraser and Swinney [28]. That is, τ_0 is set to be either the time lag that yields a local minimum of mutual information I or the time lag that reduces I to below e^{-1}.

We next divide the time series into first and second halves. The first half is used as a source for generating library dynamic patterns consisting of pairs $\mathbf{x}(t_i)$ and their corresponding future values $\Delta y_f(t_i+T\tau_0)$. At the prediction stage, we make predictions about $\mathbf{x}(t_p)$ T time steps into the future $\Delta \hat{y}_f(t_p+T\tau_0)$, which belong to the second half of the time series, using the following predictive model:

$$\Delta \hat{y}_f(t_p + T\tau_0) = \frac{\displaystyle\sum_{k=1}^{D+1} \Delta y_f(t_k + T\tau_0)\exp(-d_k)}{\displaystyle\sum_{k=1}^{D+1} \exp(-d_k)}, \tag{7}$$

$$d_k = \|\mathbf{x}(t_p) - \mathbf{x}(t_k)\|. \tag{8}$$

Here, $\mathbf{x}(t_k)(k=1,\ldots,D+1)$ represent the $D+1$ vertices of the smallest simplex that includes $\mathbf{x}(t_p)$ in the D-dimensional phase space. The prediction error can be measured in terms of the correlation coefficient between the predicted values $\Delta \hat{y}_f(t_p+T\tau_0)$ and the corresponding actual values $\Delta y_f(t_i+T\tau_0)$. Chaos causes an exponential increase in prediction error with increasing T, whereas periodic motion contaminated with external noise yields a constant prediction error independent of T.

C. Parallelness of neighboring trajectories

The long-term unpredictability of chaos appears in the form of the rapid divergence of nearby trajectories with time in phase space. However, nearby trajectories have similar directions owing to the determinism governing the time evolution that ensures short-term predictability. Thus, the diversity in the directions of neighboring trajectories is related to the degree of visible determinism in the dynamic behavior. On the basis of this fact, Kaplan and Glass [30] introduced a useful algorithm to test for determinism in a time series. This algorithm was subsequently improved by Wayland *et al.* [19] to reduce its computational burden.

Let us randomly select a vector $\mathbf{x}(t_0)$ and find its K nearest neighbors $\mathbf{x}(t_k)$ with k from 1 to K. We may set the images of all the vectors to $\mathbf{x}(t_k+T\tau_0)$ with k from 0 to K at a suitable time interval $T\tau_0$. Here, τ_0 can be determined using the prescription of Fraser and Swinney [28]. The diversity in the directions of nearby trajectories is measured in terms of the translation error E_{trans}, defined by

$$E_{trans} = \frac{1}{K+1}\sum_{k=0}^{K} \frac{\|\mathbf{v}(t_k) - \bar{\mathbf{v}}\|}{\|\bar{\mathbf{v}}\|}, \tag{9}$$

$$\bar{\mathbf{v}} = \frac{1}{K+1}\sum_{k=0}^{K} \mathbf{v}(t_k), \tag{10}$$

$$\mathbf{v}(t_k) = \mathbf{x}(t_k + T\tau_0) - \mathbf{x}(t_k). \tag{11}$$

Here, $\mathbf{v}(t_k)$ approximates the tangential vectors of the trajectories at time t_k. The more parallel the trajectories are to each other, that is, the more visible determinism there is in the time series, the closer E_{trans} will be to zero. In a previous numerical work, it was shown that a time series can be regarded as a chaotic process if $E_{trans} < 0.5$ and as a stochastic process if $E_{trans} > 0.5$ [31]. In the case of white noise, $E_{trans} \approx 1$ independent of the embedding dimension.

In estimating the translation error, we can reduce the stochastic error by obtaining the medians of E_{trans} for Q sets of M randomly chosen $\mathbf{x}(t_i)$ and then taking the mean of the Q medians. This procedure has been shown to work well [19,21,31].

D. Surrogate data method

In experiments, it is often difficult to observe the dynamic behavior of a system many times. In extreme situations, we may only be able to acquire a single time series from which we have to infer its dynamic properties. In such situations, it is very difficult, if not impossible, to evaluate the confidence interval of an estimated statistic; thus, we cannot confidently analyze the dynamic nature of the time series. The surrogate method, devised by Theiler *et al.* [22] enables us to derive useful information about the dynamic nature of a single time series.

The surrogate method begins with postulating a null hypothesis about the dynamic nature of a time series that we aim to reject. In this work, we propose the null hypothesis that the irregular components of the unstable flame represent
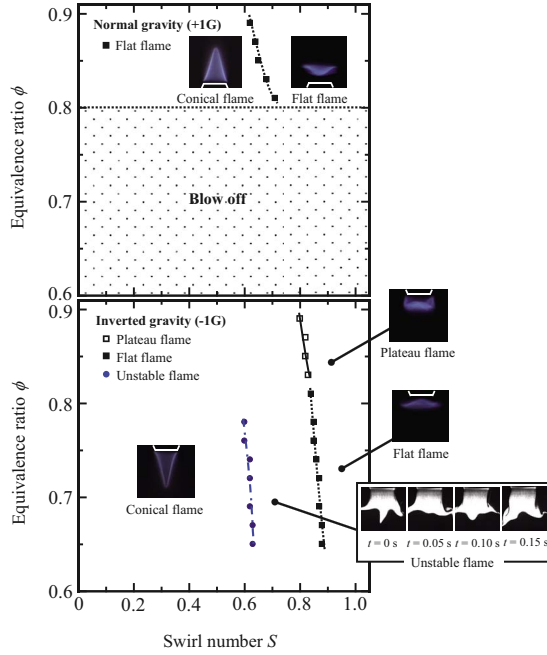
FIG. 3. (Color online) Stability maps of flame shapes of swirling flames as functions of equivalence ratio and swirl number at $U_0 = 1.0$ m/s in normal gravity ($+1G$) and inverted gravity ($-1G$).

a stochastic process; thus, the flame motion essentially consists of regular components, not chaotic ones. Under this null hypothesis, we generate twenty surrogate time series with the same power spectral structure as the original time series by applying the amplitude adjusted Fourier transform (AAFT) surrogate method [32]. In the surrogate data, the periodic components of the original data are entirely preserved, while the determinism (chaos) underlying the irregular components, if any, of the original data is completely destroyed.

The next step of the surrogate method is to estimate a statistic for both the original time series and the surrogate time series. Thus, we evaluate the difference between the values of translation error estimated for the original and the twenty surrogate time series to assess the probability of the null hypothesis being true. If the difference is sufficiently large, we can reject the null hypothesis.

IV. RESULTS AND DISCUSSION

Changes in the overall flame shapes of swirling flames in the buoyancy-dominated region ($U_0 = 1.0$ m/s, $R_e = 780$, $R_i > 0.1$) are shown in Fig. 3 as functions of equivalence ratio ϕ and swirl number S in normal gravity ($+1G$) and inverted gravity ($-1G$). The lines represent the transition boundaries between the flame shapes. In the case of normal gravity, when $\phi = 0.82$ and $S \le 0.2$, the shape of the conical flame is unaffected by swirling flow and remains unchanged. When S increases to 0.4, the flame tip starts to deviate from the rotational axis of the burner tube, and the flame height decreases. Although the deviation of the flame tip is due to the increase in the centrifugal force on the reactants, the conical shape is still maintained. Upon increasing S to 0.7, the degree of flow divergence is sufficiently large to produce

a stagnation point flow above the burner tube exit. As a result, the conical flame changes to a flat flame. With increasing ϕ, the flat flame is formed at lower value of S because it becomes easy for the flame front to propagate in the upstream direction with the increase in flame intensity. The formation regions of these flame shapes as functions of ϕ and S in normal gravity are different from those reported in our previous works [9,10], and the changes in flame shape are simples. This is because the effects of both coflow [9,10] and Taylor-like vortex motion around the burner tube exit [16] are removed in this work. In contrast to the $+1G$ case, when the orientation of the burner system relative to the gravitational direction is changed, i.e., in inverted gravity ($-1G$), the formation region of the conical flame is considerably extended with ϕ reduced to 0.64. As will be shown in images of TiO$_2$ particles visualized by the laser tomographic method (see Fig. 5), in inverted gravity the hot combustion products behind the flame front cover the entire burner tube owing to the upward buoyant force, resulting in an increase in the temperature of the burner tube in comparison with that in the case of the $+1G$ conical flame. As a result, the flame front in $-1G$ can attach to the burner rim more easily than that in $+1G$. This allows the $-1G$ conical flame to be stabilized under lower equivalence ratios. The formation region of the flat flame is also extended compared with those obtained in $+1G$. When ϕ is more than 0.83, the flat flame cannot be lifted to above the burner tube exit and the conical flame changes to a plateau flame. The most important and interesting phenomenon generated by the inversion of gravitational orientation is the formation of an unstable flame with its front switching back and forth between a stable conical flame and a stable flat flame. As shown in the time sequence images (in the inset in Fig. 3) obtained by the laser tomographic method, the flame front of this unstable flame fluctuates with a large deformation of its configuration. The important point to note for Fig. 3 is that the unstable flame is formed only under low equivalence ratios, which are sensitive to buoyancy. Similar trends for all flames can be observed even under relatively high flow velocities of up to $U_0 = 1.6$ m/s, i.e., the momentum-dominated region ($R_e = 1250$, $R_i \approx 0.04$) we studied in this work. These results indicate that the change in gravitational orientation relative to the flame front has a significant impact on the overall flame shape of swirling flames. In this work, we undertake an intensive investigation of the dynamic behavior of the unstable flame generated by the inversion of gravitational orientation.

For two representative cases of unstable flames observed in the buoyancy-dominated ($U_0 = 1.0$ m/s, $R_e = 780$, $R_i \approx 0.1$) and momentum-dominated regions ($U_0 = 1.6$ m/s, $R_e = 1250$, $R_i \approx 0.04$), the deviation from the mean value of the flame front location Δy_f as a function of time t and the power spectrum obtained by fast Fourier transform (FFT) analysis are shown in Fig. 4. In this study, the equivalence ratio of premixed reactants of $\phi = 0.68$ is selected as a representative value for investigating the dynamic behavior of flame front fluctuations. As depicted in the inset in Fig. 4, Δy_f at $U_0 = 1.0$ m/s fluctuates with time and its power spectrum exhibits a dominant peak at approximately 3.7 Hz, indicating a periodic oscillation. In addition to this
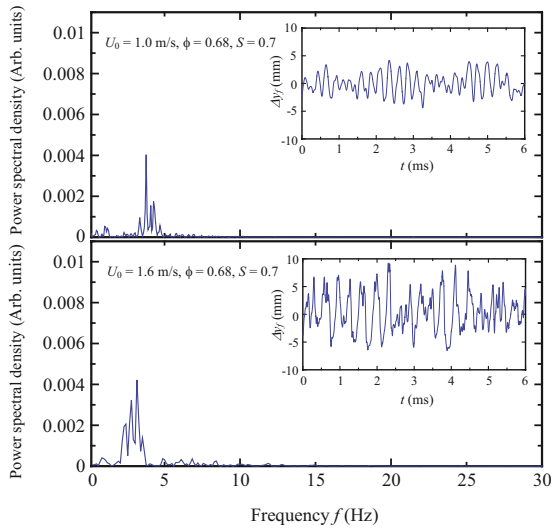
FIG. 4. (Color online) Time variation of deviation from mean value of flame front location and power spectrum.

oscillation frequency, many small peaks also appear over a range of low-frequency bands in the power spectrum. These small peaks make the dynamic behavior of Δy_f complex. Upon increasing U_0 to 1.6 m/s, the fluctuation of Δy_f becomes more complex with a larger amplitude. The power spectrum at $U_0 = 1.6$ m/s has a wider frequency distribution than that at $U_0 = 1.0$ m/s, and the power density of the oscillation frequency corresponding to that of the dominant oscillation observed at $U_0 = 1.0$ m/s still persists in the flame front dynamics. As mentioned in Sec. I, flame dynamics in inverted gravity is sensitive to the motion of the combustion products because light combustion products are formed below the heavy reactants. Therefore, it is supposed that the hydrodynamic instability associated with upward buoyancy is related to the onset of the dominant oscillation mode of the unstable flame. To reveal the relevance of buoyancy to flame dynamics, we discuss its effect on flame dynamics in inverted gravity, focusing on how the motion of combustion products changes with increasing swirl number.

Time evolutions of the combustion products in the buoyancy-dominated region ($U_0 = 1.0$ m/s, $R_e = 780$, $R_i \approx 0.1$) in inverted gravity are shown in Fig. 5. For the non swirling flame case ($S = 0$), the interface between the combustion products and the surrounding air is nearly flat around the centerline of the burner tube, and no buoyancy-induced large-scale vortical structure associated with the Kelvin-Helmholtz instability is formed at the products/air interface. As a result, the flame front does not fluctuate periodically with time, similarly to those reported in a previous paper [3]. Under low swirl conditions of up to $S = 0.3$, the particle tracks of combustion products behind the flame front are basically similar to those obtained for the non swirling flame case, and the products/air interface remains stable with time. This means that a weak swirl does not affect the motion of combustion products. Interestingly, when the unstable flame is formed at $S = 0.7$, a large-scale vortical structure appears in the hot combustion products, and the products/air interface fluctuates with time. As can be seen in the particle tracks of the combustion products for the non swirling flame case, the
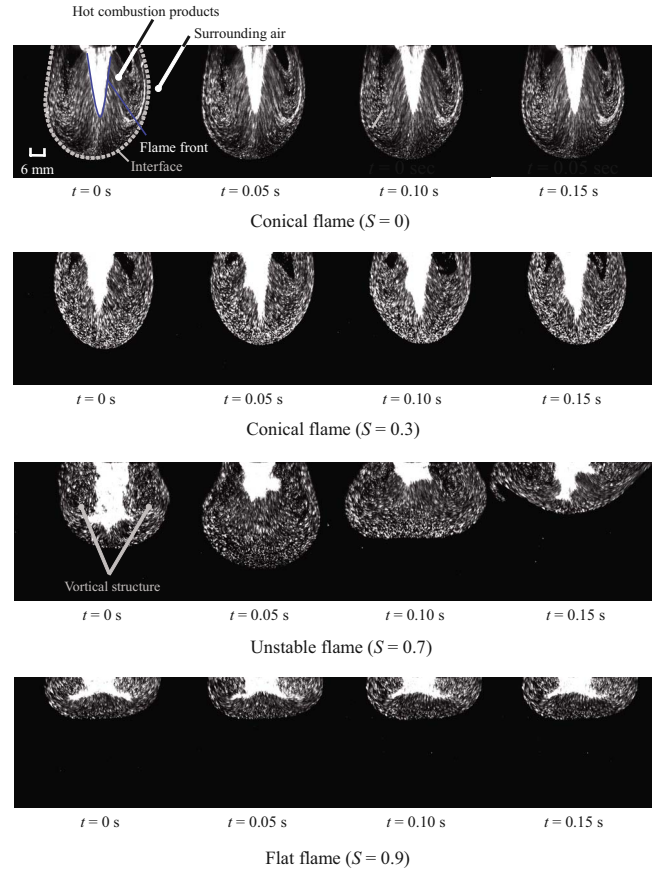
FIG. 5. (Color online) Time evolutions of products/air interface of swirling flames at $U_0 = 1.0$ m/s in inverted gravity

flow field easily becomes unstable as opposed to the normal gravity case, because a reversed flow is produced on both sides of the flame front by the upwardly accelerated flow generated by the buoyant force [5]. The outward centrifugal force produced by the swirl affects the flow field so that a large-scale toroidal vortex appears in the combustion products. As the centrifugal force increases and competes with the flow field in the combustion products, the toroidal vortex becomes unstable, which generates fluctuations of the products/air interface. Under high swirl conditions of up to $S = 0.9$ where a stable flat flame is formed, the unstable vortex motion vanishes and the products/air interface becomes stable. Time evolutions of the combustion products in the momentum-dominated region ($U_0 = 1.6$ m/s, $R_e = 1250$, $R_e \approx 0.04$) for the unstable flame in inverted gravity are shown in Fig. 6. With increasing flow momentum of the reactants, vortex breakdown in the combustion products clearly occurs, and the intermittent nature of the flow field during breakdown generates larger fluctuations of the products/air interface compared with those when $U_0 = 1.0$ m/s. The important point to note is that in normal gravity, the vortical structure and its breakdown process are not induced in the combustion products by the swirl. These observations seem to suggest that the large flow fluctuations in the combustion products generated by the vortex motion affect the unstable stratification of the flame front (dense reactants above light combustion products) in inverted grav-
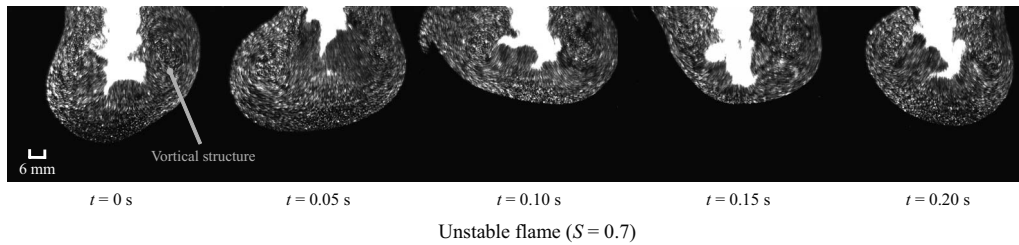
FIG. 6. Time evolutions of products/air interface of unstable flame at $U_0 = 1.6$ m/s in inverted gravity

ity and promote the deformation of the flame front owing to the hydrodynamic instability related to the Rayleigh-Taylor instability.

To conduct a more comprehensive investigation of the effect of unstable combustion products on flame front fluctuations, we investigate the time variation of fluctuations of the products/air interface. The time variation of the deviation from the mean value of the products/air interface location $\Delta y_i (= y_i - \bar{y}_i)$ as a function of time t and power spectrum are shown in Fig. 7. Here, y_i is the location of the products/air interface along the centerline of the burner tube, and $\bar{y}_i$ is the time-averaged interface location. At $U_0 = 1.0$ m/s, Δy_i regularly oscillates with time and its power spectrum has a distinct peak at approximately 3.3 Hz. This oscillation frequency is nearly in accord with that of the flame front fluctuations shown in Fig. 4. Upon increasing U_0 to 1.6 m/s, Δy_i becomes more complex, but the dominant peak at approximately 3 Hz remains in the power spectrum even in the momentum-dominated region. These low oscillation frequencies created by vortex motion are dominantly included in the power spectrum of the flame front fluctuations shown in Fig. 4. Therefore, it is conceivable that some of the low-frequency components included in the fluctuations of the flame front are mainly produced by the dynamic motion of the unstable vortical structure in upwardly moving combustion products. The physical interpretation, based on flow visualization and the time variation of the products/air interface, indicates that the unstable combustion products
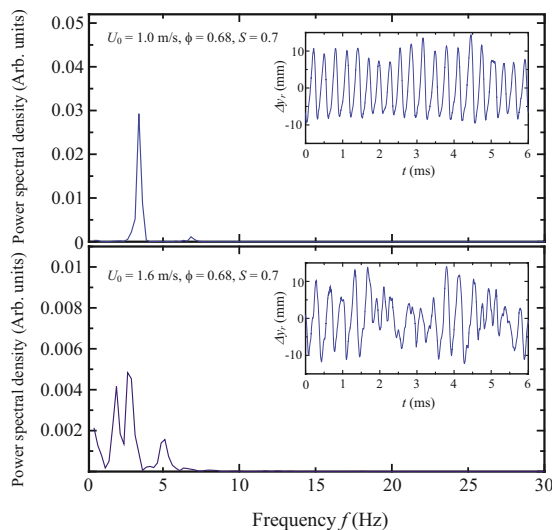
generated by the change in the buoyancy/swirl interaction in inverted gravity have a significant impact on the large fluctuations of the flame front. These results also demonstrate that it is necessary to include downstream contributions (i.e., the elliptic problem) when analyzing flame instability issues involving swirling flow. As mentioned in Sec. I, characterizing the flame front fluctuations from the viewpoint of nonlinear chaos dynamics is of importance for understanding the complex nonlinear phenomena in flame dynamics, which have not been extensively explored in the fields of combustion science and physics. Therefore, we investigate the dynamic properties of unstable flames by sophisticated nonlinear time series analysis.

Mutual information for unstable flames observed in the buoyancy-dominated and momentum-dominated regions is shown in Fig. 8 as a function of time lag τ. Here, the sampling rate of the time series is 1 kHz and the size of the data set is $n = 8,000$. In the case of $U_0 = 1.0$ m/s, the mutual information I decreases exponentially until $\tau = 60$ ms, then oscillates with a period of about 130 ms, attenuating gradually with time. The value of the period corresponds to the dominant peak observed in the power spectrum. The periodic oscillation observed in the power spectrum is dominant in flame front dynamics, but a spontaneous and exponential loss of information, which is likely to be caused by the onset of deterministic chaos, is clearly observed. Upon increasing U_0 to 1.6 m/s, the amplitude of the periodic undulation decreases and asymptotically approaches the same level as that for $U_0 = 1.0$ m/s, indicating a significant increase in dynamic instability. To investigate the characteristics of the dynamic instability that appears in the significant decay of mutual information, the short-term predictability and parallelisms of trajectories in phase space are discussed as follows.

The correlation coefficient R between the predictions and the corresponding actual values as a function of prediction

FIG. 7. (Color online) Time variation of deviation from mean value of products/air interface location and power spectrum.
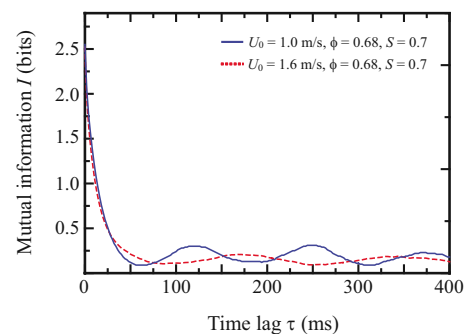
FIG. 8. (Color online) Variation in mutual information as a function of time lag.
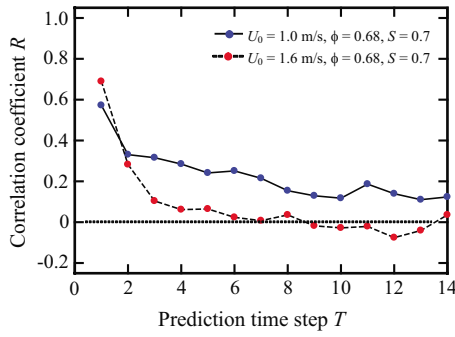
FIG. 9. (Color online) Variation in correlation coefficient (prediction error) as a function of prediction step time.

step time T, obtained by the SM algorithm [18], is shown in Fig. 9. If the dynamic behavior of the flame front is periodic, the correlation coefficient should be almost unity regardless of the prediction time step. If the dynamic behavior is nonperiodic, i.e., chaotic, the correlation coefficient should rapidly decay with increasing prediction time step. As shown in Fig. 9, R at $U_0 = 1.0$ gradually decreases to 0.1 with increasing T. This indicates that the dynamic behavior of the unstable flame in the buoyancy-dominated region represents deterministic chaos because of its short-term predictability and long-term unpredictability. At $U_0 = 1.6$ m/s, R decreases with increasing T much faster than it does at $U_0 = 1.0$ m/s, which may imply that the flame motion is more complex because of the larger degrees of freedom involved in the chaotic behavior.

The translation error E_{trans} of neighboring trajectories in phase space is estimated as a function of embedding dimension D for the original time series and AAFT surrogate data, as shown in Fig. 10. At $U_0 = 1.0$ m/s, E_{trans} for the original time series data significantly decreases with increasing D and becomes constant when D exceeds 10. The crossing of neighboring trajectories in phase space is minimal when $D \geq 10$, resulting in observable determinism similar to finite-dimensional chaos. The saturated value of E_{trans} is considerably smaller than the criterion value ($E_{trans} = 0.1$) below which determinism in the parallelism of neighboring trajectories can be said to be observable [31]. A similar trend for E_{trans} with respect to D is observed for the AAFT surrogate data. However, the translation error for the original time se-
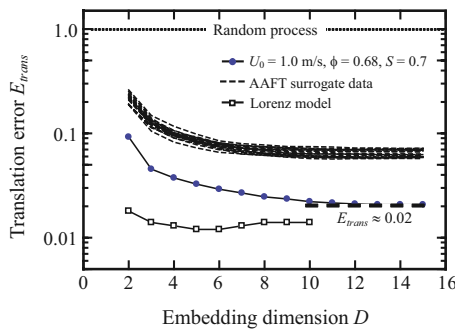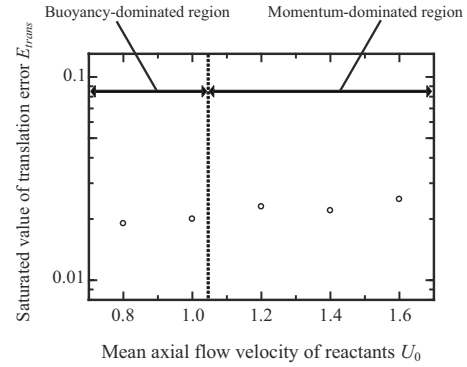
FIG. 11. Variation in saturated value of translation error as a function of mean axial flow velocity of reactants.

ries takes a significantly lower value than that for the AAFT surrogate data at each embedding dimension. In fact, the null hypothesis can be rejected by the two-sided t test of estimates of E_{trans} at 5% reliability. These results suggest that the dynamic behavior of the unstable flame observed at $U_0 = 1.0$ m/s represents deterministic chaos. The Lorenz equation [33] theoretically derived from the vorticity and energy equations under a free boundary condition, is often used in thermal and fluid physics as an important indicator for understanding the nonlinear characteristics of the dynamic instability in unstable phenomena generated by buoyancy-driven hydrodynamic instability. Although the Lorenz equation is not appropriate for representing the flame dynamics, it can be useful as an indicator for discussing the amount of complexity of the dynamic instability. The deterministic chaos produced by the Lorenz equation is treated as low-dimensional chaos, and its translation error is about 0.015. This clearly shows that the dynamic instability of flame front fluctuations can be concluded to be low-dimensional deterministic chaos. As explained previously, the results of FFT analysis and mutual information show that a periodic oscillation mode dominates the dynamic behavior of the unstable flame. On the basis of these results, the chaotic irregular fluctuation in the flame front dynamics is superimposed on the dominant periodic oscillation generated by unstable large-scale vortex motion in combustion products, resulting in low-dimensional deterministic chaos. The change in the saturated value of E_{trans} as a function of the mean flow velocity of reactants U_0 is shown in Fig. 11. In the buoyancy-dominated region, the value of E_{trans} is nearly constant. It gradually increases by a factor of 1.5 when U_0 is increased from 0.8 to 1.6 m/s, but the dynamic instability of flame front fluctuations does not switch to moderate-dimensional deterministic chaos. It is interesting to note that even in the momentum-dominated region, the low-dimensional determinism persists in flame dynamics. As shown in Fig. 7, the dynamic behavior of the products/air interface at $U_0 = 1.6$ m/s seems to be quasiperiodic oscillation. To reveal whether or not its dynamic behavior is quasiperiodic oscillation, E_{trans} for the time variation of Δy_i at $U_0 = 1.6$ m/s is shown as a function of D in Fig. 12. Note that the change in E_{trans} for quasiperiodic oscillation, defined as $y = \sin\sqrt{5}t + \sin\sqrt{7}t$, is plotted. The saturated value of E_{trans} is smaller than 0.015 which indicates the low-dimensional chaos, but is

FIG. 10. (Color online) Variation in translation error as a function of embedding dimension: original data ($\bullet$ and line) and AAFT surrogate data (lines) at $U_0 = 1.0$ m/s.
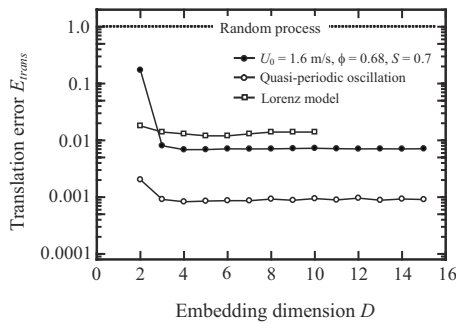
FIG. 12. Variation in translation error as a function of embedding dimension: original data (● and line) and quasiperiodic oscillation (○ and line) at $U_0 = 1.6$ m/s.

significantly larger than that of quasiperiodic oscillation ($E_{trans} \approx 0.0009$). This means that the dynamic behavior of the products/air interface at $U_0 = 1.6$ m/s is not quasiperiodic oscillation. Although it does not have the same degree of complexity as that produced by the Lorenz equations, it can be concluded that the dynamic behavior of the products/air interface at $U_0 = 1.6$ m/s is within the range of low-dimensional chaos. These results demonstrate that the dynamic behavior of unstable flames generated by the inversion of gravitational orientation relative to the flame front is low-dimensional deterministic chaos, which has not been reported in previous fundamental combustion research on swirling combustion instabilities. These results also show that the sophisticated nonlinear time series analysis we applied in this work is valid for clarifying the characteristics of complex flame instability.

V. CONCLUSIONS

The dynamic behavior of a swirling premixed flame generated by the effect of gravitational orientation has been experimentally and numerically investigated under flow conditions that span buoyancy-dominated ($R_i > 0.1$) and momentum-dominated ($R_i < 0.1$) regions. Interestingly, when the gravitational direction is changed relative to the flame front, i.e., in inverted gravity ($-1G$), an unstably fluctuating flame (unstable flame) is formed between a stable conical flame and a stable flat flame in a limited domain of equivalence ratio and swirl number. The time history of flame front fluctuations and its power spectral density show that in the buoyancy-dominated region, chaotic irregular fluctuation with low frequencies is superimposed on the dominant periodic oscillation of the unstable flame. This periodic oscillation is produced by unstable large-scale vortex motion in combustion products generated by a change in the buoyancy/swirl interaction due to the inversion of gravitational orientation, which is shown by laser tomographic visualization and the time variation of the interface location between combustion products and the surrounding air. As a result, the dynamic behavior of the unstable flame becomes low-dimensional deterministic chaos. Its dynamics maintains low-dimensional deterministic chaos even in the momentum-dominated region, in which vortex breakdown in the combustion products clearly occurs. These results were clearly demonstrated by the use, in combination with a surrogate method, of sophisticated nonlinear time series analysis, which has not been widely applied to the investigation of combustion phenomena. The analytical methods we applied in this work were shown to be valid for quantifying the dynamic properties of complex flame instability in a lean swirling premixed flame.

[1] D. Durox, F. Baillot, R. Scoufflaire, and Prudhomme, Combust. Flame **82**, 66 (1990).

[2] D. Durox, T. Yuan, F. Baillot, and J. M. Most, Combust. Flame **102**, 501 (1995).

[3] L. W. Kostiuk and R. K. Cheng, Exp. Fluids **18**, 59 (1994).

[4] L. W. Kostiuk and R. K. Cheng, Combust. Flame **103**, 27 (1995).

[5] B. Bedat and R. K. Cheng, Combust. Flame **107**, 13 (1996).

[6] R. K. Cheng, B. Bedat, and L. W. Kostiuk, Combust. Flame **116**, 360 (1999).

[7] S. Ishizuka, Prog. Energy Combust. Sci. **28**, 477 (2002).

[8] J. M. Cha and S. H. Sohrab, Combust. Flame **106**, 467 (1996).

[9] H. Gotoda, K. Maeda, T. Ueda, and R. K. Cheng, Combust. Flame **134**, 67 (2003).

[10] H. Gotoda and I. G. Shepherd, *Proceedings of 21st International Colloquium on the Dynamics of Explosions and Reactive Systems, paper 241* (Poitiers, France, 2007).

[11] G. Broze and F. Hussain, J. Fluid Mech. **263**, 93 (1994).

[12] Y. F. Dong, Z. L. Wei, and C. Xu, Phys. Fluids **9**, 2580 (1997).

[13] H. Koizumi, Int. J. Heat Mass Transfer **45**, 937 (2002).

[14] S. F. Wang, R. Mosdorf, and M. Shoji, Int. J. Heat Mass Transfer **46**, 1519 (2003).

[15] K. Nakabayashi, W. Sha, and Y. Tsuchida, J. Fluid Mech. **534**, 327 (2005).

[16] H. Gotoda, Y. Asano, K. H. Chuah, and G. Kushida, Int. J. Heat Mass Transfer **52**, 5423 (2009).

[17] P. Grassberger and I. Procaccia, Phys. Rev. Lett. **50**, 346 (1983).

[18] G. Sugihara and R. M. May, Nature (London) **344**, 734 (1990).

[19] R. Wayland, D. Bromley, D. Pickett, and A. Passamante, Phys. Rev. Lett. **70**, 580 (1993).

[20] T. Miyano, S. Munetoh, K. Moriguchi, and A. Shintani, Phys. Rev. E **64**, 016202 (2001).

[21] T. Miyano, T. Moriya, H. Nagaike, N. Ikeuchi, and T. Matsumoto, J. Phys. D **41**, 035209 (2008).

[22] J. S. Theiler, S. Eubank, A. Lonting, B. Galdrinkian, and J. D. Framer, Physica D **58**, 77 (1992).

[23] I. G. Shepherd, R. K. Cheng, and L. Talbot, Exp. Fluids **13**, 386 (1992).

[24] S. Kadowaki and N. Ohkura, Trans. Jpn. Soc. Aeronaut. Space Sci. **51**, 133 (2008).

[25] A. R. Osborne and A. Provenzale, Physica D **35**, 357 (1989).

[26] D. Ruelle, Proc. R. Soc. Lond. A Math. Phys. Sci. **427**, 241 (1990).

[27] G. A. Gottwald and I. Melbourne, Proc. R. Soc. Lond. A **460**, 603 (2003).

[28] A. M. Fraser and H. L. Swinney, Phys. Rev. A **33**, 1134 (1986).

[29] F. Takens, *Dynamical Systems of Turbulence*, Lecture Notes in Mathematics Vol. 898 (Springer, New York, 1981), p. 366.

[30] D. T. Kaplan and L. Glass, Physica D **64**, 431 (1993).

[31] T. Miyano, Int. J. Bifurcation Chaos Appl. Sci. Eng. **6**, 2031 (1996).

[32] T. Schreiber and A. Schmitz, Phys. Rev. Lett. **77**, 635 (1996).

[33] S. T. Strogatz, *Nonlinear Fynamics and Chaos* (Perseus Publishing, Cambridge, MA, 1994), Vol. 301.